Common-path Illumination in ESPI: Enhancing Sensitivity for Measuring Specular Deformation

Peizheng Yan(闫佩正)[1,2,†], Xiangwei Liu(刘向玮)[1,2,†], Xinda Zhou(周信达)[3], Rongsheng Ba(巴荣生)[3], Hanxuan Zhou(周寒萱)[1,2], Yonghong Wang(王永红)[1,2*], Jie Li(李杰)[3,4**]

[1] School of Instrument Science and Optoelectronics Engineering, Hefei University of Technology, Hefei, Anhui, 230009, China.
[2] Anhui Province Key Laboratory of Measuring Theory and Precision Instrument, Hefei University of Technology, Hefei, Anhui, 230009, China.
[3]Laser Fusion Research Center, China Academy of Engineering Physics, Mianyang 621900, China;
†These authors contributed equally to this work.
* Corresponding author: yhwang@hfut.edu.cn; ** corresponding author: ljieleej@163.com

In this study, an innovative technique is introduced to significantly enhance the sensitivity of electronic speckle pattern interferometry (ESPI) for the dynamic assessment of specular (mirrorlike) object deformations. By utilizing a common-path illumination strategy, wherein illumination and observation beams are precisely aligned, this method effectively doubles the optical path difference, leading to a twofold increase in measurement sensitivity. In addition, this method mitigates the effects of speckle noise on the measurement of minor deformations, expanding the applications of ESPI. Theoretical and experimental evaluations corroborate the efficacy of this approach.
Keywords: EPSI; common-path illumination; measurement sensitivity; specular deformation.

1. Introduction.

High-sensitivity material measurement is critically important in many sectors, such as biomedicine, automotive, and aerospace[1, 2]. Traditional strain gauges, which are limited by their point measurement nature, are inadequate in certain applications, such as in ultra-smooth optical components[3] or plasma interactions[4]. Optical interferometric measurement, recognized for its full-field, noncontact, and real-time capabilities, is currently a prevalent method in modern industries[5]. In particular, electronic speckle pattern interferometry (ESPI) is widely applied due its ability to obtain deformation information directly with high accuracy and simplicity in optical path setup[6-8].

ESPI obtains object deformation by measuring the phase difference of the speckle field on the surface of an object before and after deformation. For specular objects, the relationship between phase difference Δ and out-of-plane deformation d is $\Delta = 4\pi d\cos\alpha/\lambda$[9], where α is the angle between the illumination light and the object's normal, and λ is the coherent light's wavelength. Given the low value of λ, even submicron deformations can produce large phase values. However, its application encounters obstacles when measuring extremely small deformations, such as the thermal deformation of certain high-precision optical elements. These materials typically exhibit phase changes that are inadequate to generate discernible interference fringes. A critical issue is that ESPI's measurement principal hinges on detecting phase changes within the speckle field, and thus, significant speckle noise is frequently present in the resultant speckle fringe images, which can obscure the measurement phase, affecting the accuracy of measurements or potentially leading to measurement errors. Notably, limited research has focused on enhancing the sensitivity of speckle interferometry measurements. Previous studies, such as those conducted by Sohmer, explored methods to amplify in-plane measurement sensitivity[10-12]. However, these techniques tend to be complex, offer a limited field of view, and do not address the enhancement of sensitivity in out-of-plane deformation measurements.

In the current study, we introduce an advanced dynamic measurement method for specular objects by using common-path illumination in ESPI. By coaxially aligning illumination and observation beams, our method achieves a twofold increase in optical path difference compared with traditional techniques, substantially enhancing detection sensitivity.

2.Principle.

Fig. 1 illustrates the optical path configuration of our common-path illumination ESPI system designed for specular object measurement. The system begins with a laser source, the output of which is directed into the measurement setup via a mirror (M1). The beam expander (BE) and pinhole (PH1) collaboratively expand and spatially filter the incident light. This light is subsequently divided by the beam splitter (BS1) into two paths: the transmitted light is the object light, and the reflected light is the reference light. The object light diverges via the projection lens (PL) and then reflected onto the specular object by the polarizing plate beam splitter (PPBS), becoming the illumination light. The half-wave plate (HWP1) adjusts the beam polarization state, such that the illumination light can be completely reflected by PPBS, improving light utilization. The specular object is positioned at a set angle relative to the measurement system, directing

the illumination light onto a rough surface located on the opposite side. This setup ensures that the illumination light generates the requisite speckle patterns for ESPI. The rough surface needs to completely take up the light reflected from the specular object, which requires the area of the rough surface to be slightly larger than the specular object. When the angle is smaller, the rough surface will be closer to the imaging optical axis of the system, in order to avoid the imaging field of view is obscured, the angle cannot be too small, its value needs to be determined according to the size of the specular object and the system space. A portion of the diffusely reflected light, which now serves as the observation light, is then reflected back toward the measurement system by the specular object. The observation light is spectrally constrained by PH2 and focused onto the image sensor by the imaging lens (IL) and BS2. The reference light is recollimated through the collimating lenses (CL1, CL2), and its diameter and direction are further refined by PH3 and M2. Finally, the reference light interferes with the object light in the image sensor. Given the longer propagation path and multiple refractions of the object light, its intensity is significantly lower than that of the reference light. To achieve better interference effects, a neutral density filter (NDF) is used to reduce the intensity of the reference light to near that of the object light. Then, a combination of adjustments to HWP2 and the linear polarizer (LP) is implemented to achieve the optimal ratio of light intensities, enhancing the contrast of the interference fringes. The conditions for the spatial carrier phase extraction method are met by adjusting the size of PH2 to constrain the spectrum of object light and adjusting M2 to control the direction and magnitude of the introduced spatial carrier frequency in reference light, enabling dynamic measurement[13].

Fig. 2(a) presents a detailed schematic representation of the optical trajectory at a designated point F on a specular object before and after deformation in the measurement system. The illumination light originates from point I, extending along IF, and forming an angle α with the normal to the specular surface. Upon reflection by the specular surface, this illumination beam undergoes diffuse reflection off a relatively positioned rough surface, as delineated in Fig. 2(b). Subsequently, a portion of this diffusely scattered light is retro-reflected by the specular object, culminating in the formation of the observation beam, as depicted in Fig. 2(c). By symmetrically positioning the focal point of the projection lens (FPL) and PH2 relative to PPBS, and utilizing the principle of reversibility in light propagation, the locations of FPL and PH2 equivalently mirror that of the illumination source. Such a symmetrical arrangement ensures that the observation and illumination beams follow an identical optical path, maintaining congruency in their trajectories.

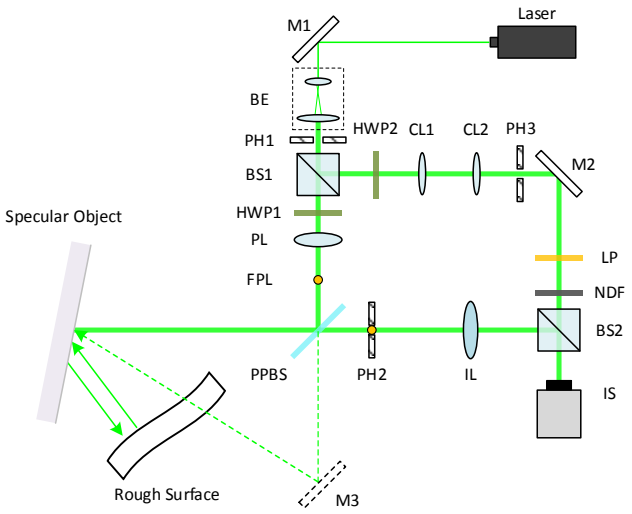

Fig. 1. Schematic of the common-path illumination speckle interferometry for specular object deformation measurement. M, mirror; BE, beam expender; PH, pinhole; BS, beam splitter; HWP, half-wave plate; PL, projector lens; FPL, focal point of the projection lens; PPBS, polarizing plate beam splitter; IL, imaging lens; CL, collimating lens; LP, linear polarizer; NDF, neutral density filter; IS, image sensor.

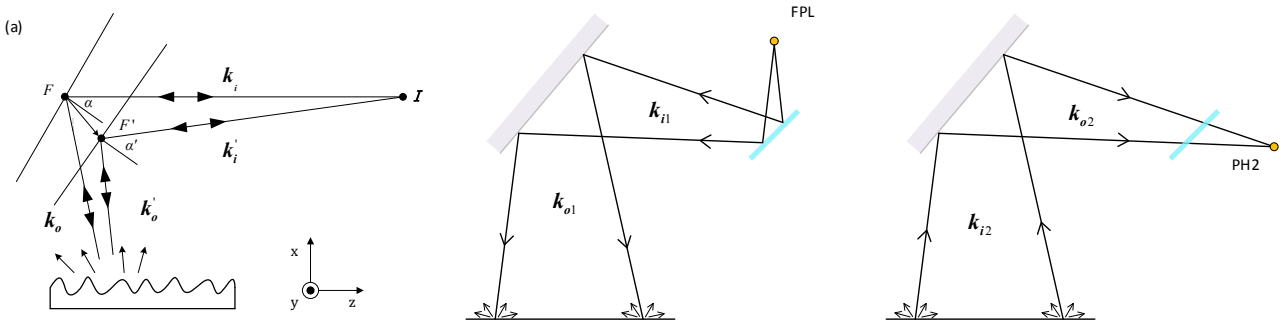

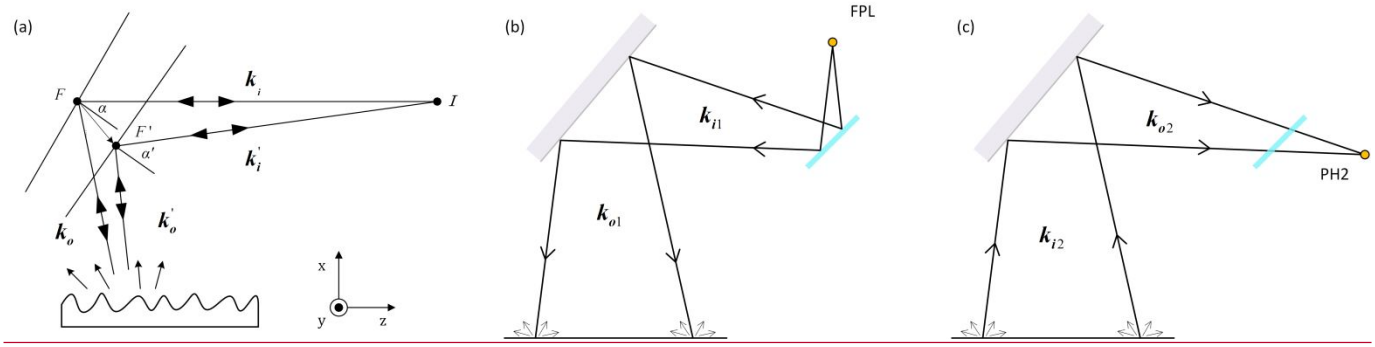

Fig. 2. (a) Schematic of the light path for a point on the specular object before and after deformation in the measurement system. (b) Schematic of the illuminated beam being reflected by a specular object. (c) Schematic of the observation beam being reflected by a specular object.

Subsequent to the deformation of the specular object, the designated point F transitions into F", and the incident angle between the illumination light and the object's normal shifts from α to α'. Considering the double reflection of the object light by the specular surface, the relationship between out-of-plane deformation $\boldsymbol{d}$ and the resulting phase difference $\boldsymbol{\delta}$ can be expressed as follows:

$$\boldsymbol{\delta} = \boldsymbol{d} \cdot 2\boldsymbol{K}, \tag{1}$$

where $\boldsymbol{K}$ is the sensitivity vector of deformation determined by the difference between the incident wave vector $\boldsymbol{k}_1$ and the reflected wave vector $\boldsymbol{k}_o$[9], which is:

$$\boldsymbol{K} = \boldsymbol{k}_0 - \boldsymbol{k}_i. \tag{2}$$

The specular object does not undergo in-plane deformation, and thus, the sensitivity vector $\boldsymbol{k}$ is parallel to the mirror normal $\hat{\boldsymbol{n}}$. In accordance with the law of reflection, we have

$$\boldsymbol{k}_0 \cdot \boldsymbol{K} = -\boldsymbol{k}_i \cdot \boldsymbol{K}. \tag{3}$$

By combining Eq. 2 and 3, rewriting the sensitivity vector $\boldsymbol{K}$ as $\boldsymbol{K} = K\hat{\boldsymbol{n}}$, and expanding $\boldsymbol{k}_o$ as $\boldsymbol{k}_o = 2\pi\hat{\boldsymbol{k}}_o/\lambda$, the following is obtained:

$$\boldsymbol{K} = \frac{4\boldsymbol{\pi}}{\boldsymbol{\lambda}}\left(\hat{\boldsymbol{k}}_0 \cdot \hat{\boldsymbol{n}}\right)\hat{\boldsymbol{n}}, \tag{4}$$

where $\hat{\boldsymbol{k}}_o$ is the unit vector in the direction of the reflected wave. Furthermore, the out-of-plane deformation of the specular object is sufficiently minor to justify the assumption that the angle of incidence remains approximately constant pre- and post-deformation, denoted as $\alpha \approx \alpha'$. By substituting Eq. 4 into Eq. 1, sensitivity can be finally obtained as follows:

$$\boldsymbol{\delta} = 2\frac{4\boldsymbol{\pi}}{\boldsymbol{\lambda}}\left(\hat{\boldsymbol{k}}_0 \cdot \hat{\boldsymbol{n}}\right)\left(\hat{\boldsymbol{n}} \cdot \boldsymbol{d}\right), \tag{5}$$

where $\hat{n} \cdot d$ represents the out-of-plane deformation d of the specular surface in the normal direction. Given that the deformation of the specular surface is minimal, the angle before and after deformation can be considered unchanged, i.e., $\alpha \approx \alpha'$. Therefore, $\hat{\boldsymbol{k}}_o \cdot \hat{\boldsymbol{n}} = \cos\alpha$, and Eq. 5 can be rewritten as follows:

$$\delta = 2\frac{4\pi}{\lambda} d\cos\alpha. \tag{6}$$

The sensitivity factor $S = 8\pi\cos\alpha/\lambda$ is defined. It shows that measurement sensitivity is doubled compared with the traditional speckle interferometry techniques for mirror measurement.

Achieving precise and controllable out-of-plane deformation is challenging; hence, a high-precision rotating stage is utilized in the experiment to induce equivalent out-of-plane deformation through rotation. In this situation, the relationship between out-of-plane deformation d and rotation angle θ is as follows[14]:

$$d = \theta r, \tag{7}$$

where r is the surface coordinate of the object being measured. In the experiment, the rotation of the object is confined solely to the x-plane; therefore, the aforementioned equation can be simplified into $d = \theta x$. By substituting this into Eq. 6 and taking the partial derivatives of both sides in the x-direction, the expression for θ can be obtained as

$$\theta = \frac{\lambda}{8\pi}\frac{1}{\cos\alpha}\cdot\frac{\partial\delta}{\partial x} = \frac{1}{S}\cdot\frac{\partial\delta}{\partial x}, \tag{8}$$

where α and θ are constant values in a single measurement. Therefore, Eq. (8) shows that the phase that corresponds to

the deformation should form a plane with a fixed slope, and straight fringes are formed in the y-direction after phase wrapping. The wrapped phase is obtained using a phase extraction algorithm, and then unwrapped and fitted with a straight line along the x-direction. The slope of the fitted line is $\partial\delta / \partial x$ $\partial\square/\partial\square$, and $\square$ θ can be read out by the rotating stage. Finally, measurement sensitivity $\square$ can be calculated.

3.Experiment.

To assess the enhanced sensitivity of the proposed technology for measuring specular objects, a series of validation and comparative experiments was conducted. The object used for measurement in these experiments was a microcrystalline glass flat panel ~~sphere~~ with a diameter of 90 mm, coated with a dielectric film on its surface. The microcrystalline glass is securely mounted onto the rotating stage by using mechanical fixtures. The rotating stage's design resolution is 0.174 micro-radians, which aptly satisfies the requirements of the experiment. For imaging, an industrial camera MER2-501-79U3M from Daheng Imaging Co., with a resolution of 2448 × 2048 pixels ~~and a pixel size of 2.74 μm~~, is utilized. Optical components and mechanical parts are sourced from Lbtek Optics Co. The experiment also incorporates a rough surface, which is made of a semi-transparent acrylic board.

The experimental procedure is structured as follows: Initially, the rotation stage is moved to a predetermined point, where its current reading is recorded as the reference point and a speckle interferogram is captured as the baseline frame. Subsequently, the stage undergoes incremental rotations in steps of 1 s each. The servo motor may not achieve exact positioning due to the brevity of these steps; hence, a speckle interferogram is captured after each rotation and the stage's current reading is noted. This rotation sequence is repeated multiple times to ensure accuracy and consistency in measurements. The phase information in the speckle interferogram can be obtained using the Fourier transform method[13] and the phase map is filtered using the windowed Fourier filtering algorithm[15]. The phase difference δ relative to different rotation angles from the reference point can be obtained by subtracting the current phase map from the baseline phase map. Concurrently, the readings from the rotating stage at various instances are compared with the reference point to calculate the corresponding rotation angles. In accordance with the known phase and rotation angle, combined with Eq. 8, measurement sensitivity under the predetermined point can be obtained. The same measurement process is conducted under different predetermined points, and the experimental results are compared with a cosine curve normalized to standard sensitivity, as shown in Fig. 3(a). The measurement results are highly coincident with the cosine curve, verifying the correctness of the above theoretical derivation.

Notably, as the rotating stage moves to different predetermined points, the area within the speckle interferogram that is occupied by the specular object changes; a larger reference point degree results in a smaller area. Figs. 3(b) and 3(c) illustrate the speckle interferograms at 17° and 47°, respectively. At 47°, the area of the object becomes a narrow ellipse. Nevertheless, the "short axis" in the x-direction still corresponds to the actual radius length, as indicated by a red scale in the figure. For gradient calculation of the phase map, pixel coordinates must be converted into actual coordinates. This step requires determining a scale factor, which can be calculated by measuring the number of pixels along the short axis. The process begins with using the Canny operator for edge detection on the speckle interferogram to identify the area occupied by the object. Subsequently, the detected edges are dilated and eroded using the same parameters, assigning the occupied area as 1. The eroded image is then summed along the x-direction, and the row with the maximum value is identified as the location of the short axis. The gradient is calculated by determining the coordinates of the first and last nonzero values in this row, establishing the number of pixels occupied by the short axis, from which the scale factor is derived.

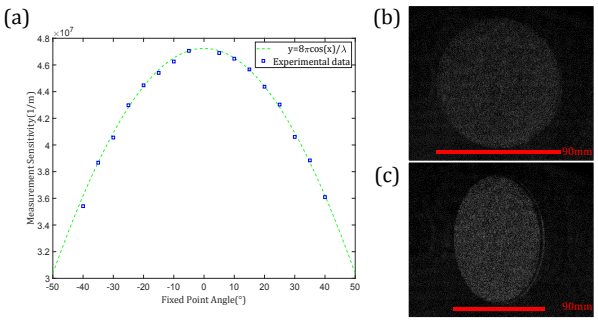

Fig. 3. (a) Comparison of experimental results with theoretical values. Speckle interferogram collected at a rotation stage reading of 17°(b) and 47°(c).

To further demonstrate the sensitivity enhancement of the proposed method, we compared it with conventional off-axis illumination techniques. The experiment involved rotating the stage to a predetermined 15° point to capture the light reflected from the specular object onto the rough surface. The PPBS is removed and a reflector M3 is placed at the dashed position in Fig. 1, where the object light is reflected by M3 and then transmitted through the rough surface to illuminate the measurement object., implementing traditional off-axis specular object detection. The optical path structure is similar to that in Ref. [16], but the one in reference performs shearography experiments. Other experimental conditions, such as the rotating stage's position, remained unchanged to preserve the integrity of the comparison. The procedure for traditional specular object detection was identical to the described method.

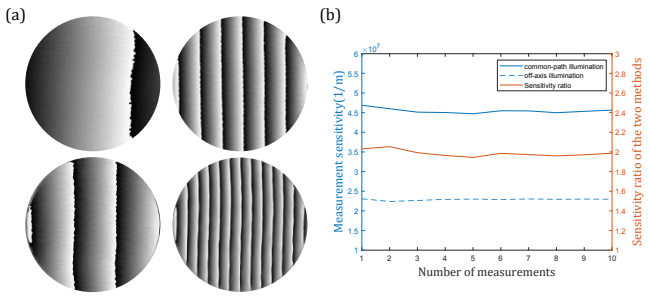

Fig. 4. (a) Phase fringe maps obtained by off-axis and common-path illumination. (b) Measurement sensitivity of two illumination methods.

Fig. 4(a) depicts the phase fringe maps captured under identical deformation by using off-axis illumination (top row) and common-path illumination (bottom row). The left column corresponds to a rotation angle of 0.00022°, while the right column is 0.00109°. A distinct observation from these maps is the denser fringe pattern in common-path illumination compared with off-axis illumination, indicating higher sensitivity. Fig. 4(b) shows the sensitivity of the two illumination methods under multiple measurements and their ratios. The sensitivity of common-path illumination is nearly exactly two times that of off-axis illumination, fluctuating only slightly with measurement noise.

Finally, to verify the effectiveness of the specular inspection system proposed in this study in detecting the real out-of-plane deformation, the microcrystalline glass used above was loaded with out-of-plane ejector pins at three different points, the predetermined α is 16°, and the results are shown in the following figure, which shows that the inspection system clearly detects the deformation at three different points.

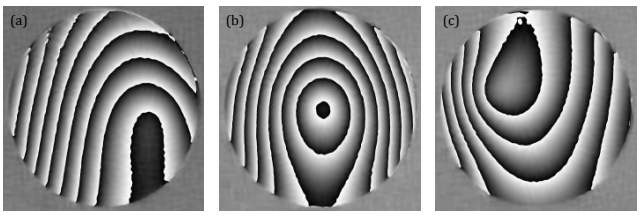

Fig. 5. Phase fringe maps obtained by ejector loading at the lower right (a), middle (b), and upper left (c) of the microcrystalline glass.

4. Conclusion

In conclusion, this research presents a highly sensitive method for measuring the deformation of specular objects. By utilizing a common-path illumination design, this technique effectively doubles the optical path difference caused by deformation, achieving two times measurement sensitivity compared with traditional methods. Detailed theoretical derivation and sufficient experiments have proved the validity of the technique. This advancement is essential for the precise assessment of optical component deformations, significantly enhancing the practical applicability of ESPI in industrial measurement scenarios.

Acknowledgements

This work was supported by National Natural Science Foundation of China (No. 52375536 and 52375535), and the Key Research and Development Program of Jiangxi Province (No. 20223BBE51010).

References

1.Y. W. Zhu, Z. K. Chen, W. J. Zhou, Y. J. Yu, and V. Tornari, "Photoacoustic speckle pattern interferometry for detecting cracks of different sizes," Optics Express **31,** 40328 (2023).

2.M. Z. Yu, C. Jia, X. G. Han, Y. Xia, L. B. Zhao, P. Yang, D. J. Lu, Y. L. Wang, X. Z. Wang, and Z. D. Jiang, "Ultra-high-sensitivity micro-accelerometer achieved by pure axial deformation of piezoresistive beams," Measurement Science and Technology **34,** 125159 (2023).

3.S. J. Li, Y. T. Huang, F. Y. Zhao, C. Yang, J. Zhang, H. F. Liang, C. L. Cai, and W. G. Liu, "Establishment and analysis of feasibility evaluation system and ultra-precision manufacturing technology for small aperture free-form surface optical element," International Journal of Advanced Manufacturing Technology **127,** 2299 (2023).

4.X. Q. Cui, H. B. Wang, M. G. Zhao, G. N. Luo, and H. B. Ding, "The measurement of plasma-facing materials' topography variation by means of temporal phase-shifting speckle interferometry technique," Nuclear Materials and Energy **12,** 1236 (2017).

5.S. Q. Liu, F. H. Yu, R. Hong, W. J. Xu, L. Y. Shao, and F. Wang, "Advances in phase-sensitive optical time-domain reflectometry," Opto-Electronic Advances **5,** 200078 (2022).

6.A. Ettemeyer, "Combination of 3-D deformation and shape measurement by electronic speckle-pattern interferometry for quantitative strain- stress analysis," Optical Engineering **39,** 212 (2000).

7.M. P. Georges, C. Thizy, F. Languy, and J. F. Vandenrijt, "An overview of interferometric metrology and NDT techniques and applications for the aerospace industry," Proceedings of the SPIE **9960,** 996007 (2016).

8.E. H. Nosekabel, T. Ernst, and W. Haefker, "Measurement of the thermal deformation of a highly stable antenna with pulse ESPI," Proceedings of the SPIE - The International Society for Optical Engineering **6616,** 66162X (2007).

9.R. S. Hansen, "A compact ESPI system for displacement measurements of specular reflecting or optical rough surfaces," Optics and Lasers in Engineering **41,** 73 (2004).

10.C. Joenathan, A. Sohmer, and L. Burkle, "Increased sensitivity to in-plane displacements in electronic speckle pattern interferometry," Applied optics **34,** 2880 (1995).

11.A. Sohmer and C. Joenathan, "Twofold increase in sensitivity with a dual-beam illumination arrangement for electronic speckle pattern interferometry," Optical Engineering **35,** 1943 (1996).

12.B. Bhaduri, M. P. Kothiyal, and N. K. Mohan, "Digital speckle pattern interferometry (DSPI) with increased sensitivity: Use of spatial phase shifting," Optics Communications **272,** 9 (2007).

13.B. Bhaduri, N. K. Mohan, M. P. Kothiyal, and R. S. Sirohi, "Use of spatial phase shifting technique in digital speckle pattern interferometry (DSPI) and digital shearography (DS)," Optics Express **14,** 11598 (2006).

14.R. S. Hansen, "Deformation measurements of specularly reflecting objects using holographic interferometry with diffuse illumination," Optics and Lasers in Engineering **28,** 259 (1997).

15.Q. Kemao, "Applications of windowed Fourier fringe analysis in optical measurement: A review," Optics and Lasers in Engineering **66,** 67 (2015).

16.P. Z. Yan, Y. Wang, F. Y. Sun, Y. Lu, L. Liu, and Q. H. Zhao, "Shearography for non-destructive testing of specular reflecting objects using scattered light illumination," Optics and Laser Technology **112,** 452 (2019).